1   # Far-UVC light: A new tool to control the spread of airborne-mediated microbial

2   # diseases

3   David Welch,* Manuela Buonanno, Veljko Grilj, Igor Shuryak, Connor Crickmore, Alan W. Bigelow,

4   Gerhard Randers-Pehrson, Gary W. Johnson & David J. Brenner

5   Center for Radiological Research, Columbia University Medical Center, New York, New York 10032,
6   USA

7   *   Correspondence   and   requests   for   material   should   be   addressed   to   D.W.
8   (email: dw2600@cumc.columbia.edu).

9   *Note: This is a preprint. This work has not been peer-reviewed.*

10

11   **Abstract**

12   Airborne-mediated microbial diseases such as influenza and tuberculosis represent major public

13   health challenges. A direct approach to prevent airborne transmission is inactivation of airborne

14   pathogens, and the airborne antimicrobial potential of UVC ultraviolet light has long been established;

15   however, its widespread use in public settings is limited because conventional UVC light sources are

16   both carcinogenic and cataractogenic. By contrast, we have previously shown that far-UVC light (207-

17   222 nm) efficiently kills bacteria without harm to exposed mammalian skin. This is because, due to its

18   strong absorbance in biological materials, far-UVC light cannot penetrate even the outer (non living)

19   layers of human skin or eye; however, because bacteria and viruses are of micrometer or smaller

20   dimensions, far-UVC can penetrate and inactivate them. We show for the first time that far-UVC

21 efficiently kills airborne aerosolized viruses, a very low dose of 2 mJ/cm^2 of 222-nm light inactivating

22 >95% of aerosolized H1N1 influenza virus. Continuous very low dose-rate far-UVC light in indoor

23 public locations is a promising, safe and inexpensive tool to reduce the spread of airborne-mediated

24 microbial diseases.

25

26   Airborne-mediated microbial diseases represent one of the major challenges to worldwide public

27   health[1]. Common examples are influenza[2], appearing in seasonal[3] and pandemic[4] forms, and bacterially-

28   based airborne-mediated diseases such as tuberculosis[5], increasingly emerging in multi-drug resistant

29   form.

30   A direct approach to prevent the transmission of airborne-mediated disease is inactivation of the

31   corresponding airborne pathogens, and in fact the airborne antimicrobial efficacy of ultraviolet (UV)

32   light has long been established[6-8]. Germicidal UV light can also efficiently kill both drug-sensitive and

33   multi-drug-resistant bacteria[9], as well differing strains of viruses[10]. However, the widespread use of

34   germicidal ultraviolet light in public settings has been very limited because conventional UVC light

35   sources are a human health hazard, being both carcinogenic and cataractogenic[11,12].

36   By contrast, we have earlier shown that far-UVC light generated by filtered excimer lamps

37   emitting in the 207 to 222 nm wavelength range, efficiently kills drug-resistant bacteria, without

38   apparent harm to exposed mammalian skin[13-15]. The biophysical reason is that, due to its strong

39   absorbance in biological materials, far-UVC light does not have sufficient range to penetrate through

40   even the outer layer (stratum corneum) on the surface of human skin, nor the outer tear layer on the

41   outer surface of the eye, neither of which contain living cells; however, because bacteria and viruses are

42   typically of micron or smaller dimensions, far-UVC light can still efficiently traverse and inactivate

43   them[13-15].

44   The earlier studies on the germicidal efficacy of far UVC light[13,15-18] were performed exposing

45   bacteria irradiated on a surface or in suspension. In that a major pathway for the spread of influenza A is

46   aerosol transmission[3], we investigate for the first time the efficacy of far-UVC 222-nm light for

47   inactivating airborne viruses carried by aerosols – with the goal of providing a potentially safe

48   alternative to conventional 254-nm germicidal lamps to inactivate airborne microbes.

Results

Virus inactivation. Fig. 1 shows representative fluorescent 40x images of mammalian epithelial cells incubated with airborne viruses that had been exposed in aerosolized form to far-UVC doses (0, 0.8, 1.3 or 2.0 mJ/cm^2) generated by filtered 222-nm excimer lamps. Blue fluorescence was used to identify the total number of cells in a particular field of view, while green fluorescence indicated the integration of live influenza A (H1N1) viruses into the cells. Results from the zero-dose control studies (Fig. 1, top left) confirmed that the aerosol irradiation chamber efficiently transmitting the aerosolized viruses through the system, after which the live virus efficiently infected the test mammalian epithelial cells.

Fig. 2 shows the surviving fraction, as a function of the incident 222-nm far-UVC dose, of exposed H1N1 aerosolized viruses, as measured by the number of focus forming units in incubated epithelial cells relative to unexposed controls. Linear regressions (see below) showed that the survival results followed a classical exponential UV disinfection model with rate constant k=1.8 cm^2/mJ (95% confidence intervals 1.5-2.1 cm^2/mJ). The overall model fit was good, with a coefficient of determination, R^2= 0.95, which suggests that most of the variability in virus survival was explained by the exponential model. The rate constant of 1.8 cm^2/mJ corresponds to an inactivation cross-section (dose required to kill 95% of the exposed viruses) of D$_{95}$ = 1.6 mJ/cm^2 (95% confidence intervals 1.4-1.9 mJ/cm^2).

Discussion

We have developed an approach to UV-based sterilization using single-wavelength far-UVC light generated by filtered excilamps, which selectively inactivate microorganisms, but does not produce biological damage to exposed mammalian cells and tissues[13-15]. The approach is based on biophysical

4

71   principles in that far-UVC light can traverse and therefore kill bacteria and viruses which are typically

72   micrometer dimensions or smaller, whereas due to its strong absorbance in biological materials, far-

73   UVC light cannot penetrate even the outer dead-cell layers of human skin, nor the outer tear layer on the

74   surface of the eye.

75   Here we applied this approach to test the efficacy of the 222-nm far-UVC light to kill influenza

76   A virus (H1N1) carried by aerosols in a benchtop aerosol UV irradiation chamber, which generated

77   aerosol droplets of sizes similar to those generated by human coughing and breathing. Aerosolized

78   viruses flowing through the irradiation chamber were exposed to UVC emitting lamps placed in front of

79   the chamber window.

80   As shown in Fig. 2, killing of influenza A virus (H1N1) by 222-nm far-UVC light follows a

81   typical exponential disinfection model, with an inactivation cross-section of $D_{95} = 1.6$ mJ/cm^2 (95% CI:

82   1.4-1.9). For comparison, using a similar experimental arrangement, but using a conventional 254 nm

83   germicidal UVC lamp, McDevitt *et al.*[19] found a D_{95} value of 1.1 mJ/cm^2 (95% CI: 1.0-1.2) for H1N1

84   virus. Thus as we[13,15] and others [16-18] reported in earlier studies for bacterial inactivation, 222-nm far-

85   UVC light and 254-nm broad-spectrum germicidal light are quite similar in their efficiencies for viral

86   inactivation, the comparatively small differences presumably reflecting differences in nucleic acid

87   absorbance. However as discussed above, based on biophysical considerations and in contrast to the

88   known human health safety issues associated with conventional germicidal 254-nm broad-spectrum

89   UVC light, far-UVC light does not appear to be cytotoxic to exposed human cells and tissues *in vitro* or

90   *in vivo*[13-15].

91   If these results are confirmed in other scenarios, it follows that the use of overhead low-level far-

92   UVC light in public locations may represent a safe and efficient methodology for limiting the

93   transmission and spread of airborne-mediated microbial diseases such as influenza and tuberculosis. In

94   fact the potential use of ultraviolet light for airborne disinfection is by no means new, and was first

95   demonstrated more than 80 years ago[8,20]. As applied more recently, airborne ultraviolet germicidal

96   irradiation (UVGI) utilizes conventional germicidal UVC light in the upper part of the room, with

97   louvers to prevent direct exposure of potentially occupied room areas[21]. This results in blocking more

98   than 95% of the UV radiation exiting the UVGI fixture, with substantial decrease in effectiveness[22]. By

99   contrast, use of low-level far-UVC fixtures, which are potentially safe for human exposure, could

100   provide the desired antimicrobial benefits without the accompanying human health concerns of

101   conventional germicidal lamp UVGI.

102   A key advantage of the UVC based approach, which is in clear contrast to vaccination

103   approaches, is that UVC light is likely to be effective against all airborne microbes. For example, while

104   there will almost certainly be variations in UVC inactivation efficiency as different influenza strains

105   appear, they are unlikely to be large[7,10]. Likewise, as multi-drug-resistant variants of bacteria emerge,

106   their UVC inactivation efficiencies are also unlikely to change greatly[9].

107   Finally it is of course by no means the case that all microbes are harmful, and it is well

108   established that the human microbiome is essential to human health[23]. With the exception of a subset of

109   the skin microbiome, all the human microbiome would be entirely shielded from far-UVC light due to

110   its very short range; in fact even within the skin biome only those biota on the skin surface[24] would be

111   potentially affected, which are of course the same biota that are potentially removed by hand

112   sanitizers[25].

113   In conclusion, we have shown for the first time that very low doses of far-UVC light efficiently

114   kill airborne viruses carried by aerosols. For example, a very low dose of 2 mJ/cm^2 of 222-nm light

115   inactivates >95% of airborne H1N1 virus. Our results indicate that far-UVC light is a powerful and

116   inexpensive approach for prevention and reduction of airborne viral infections without the human health

117   hazards inherent with conventional germicidal UVC lamps. If these results are confirmed in other

118   scenarios, it follows that the use of overhead very low level far-UVC light in public locations may

119   represent a safe and efficient methodology for limiting the transmission and spread of airborne-mediated

120   microbial diseases. Public locations such as hospitals, doctors' offices, schools, airports and airplanes

121   might be considered here. This approach may help limit seasonal influenza epidemics, transmission of

122   tuberculosis, as well as major pandemics.

123

Methods

125   **Far-UVC lamps.** We used a bank of three excimer lamps containing a Kr-Cl gas mixture that

126   predominantly emits at 222 nm [26,27]. The exit window of each lamp was covered with a custom bandpass

127   filter designed to remove all but the dominant emission wavelength as previously described[15]. Each

128   bandpass filter (Omega Optical, Brattleboro, VT) had a center wavelength of 222 nm and a full width at

129   half maximum (FWHM) of 25 nm and enables >20% transmission at 222 nm. A UV spectrometer

130   (SPM-002-BT64, Photon Control, BC, Canada) with a sensitivity range between 190 nm and 400 nm

131   was utilized to verify the 222 nm emission spectrum. A deuterium lamp standard with a NIST-traceable

132   spectral irradiance (Newport Model 63945, Irvine, CA) was used to radiometrically calibrate the UV

133   spectrometer.

134   **Far-UVC dosimetry.** Optical power measurements were performed using an 818-UV/DB low-power

135   UV enhanced silicon photodetector with an 843-R optical power meter (Newport, Irvine, CA).

136   Additional dosimetry to determine the uniformity of the UV exposure was performed using far-UVC

137   sensitive film as described in our previous work[28,29]. This film has a high spatial resolution with the

138   ability to resolve features to at least 25 µm, and exhibits a nearly ideal cosine response[30,31].

139 Measurements were taken between experiments therefore allowing placement of sensors inside the

140 chamber.

141 A range of far-UVC exposures, from 3.6 µJ/cm^2 up to 281.6 mJ/cm^2, were used to define a

142 response calibration curve. Films were scanned as 48 bit RGB TIFF images at 150 dpi using an Epson

143 Perfection V700 Photo flatbed scanner (Epson, Japan) and analyzed with radiochromic film analysis

144 software[32] to calculate the total exposure based on measured changes in optical density.

145 Measurements using both a silicon detector and UV sensitive films were combined to compute

146 the total dose received by a particle traversing the exposure window. The three vertically stacked lamps

147 produced a nearly uniform dose distribution along the vertical axis thus every particle passing

148 horizontally through the irradiation chamber received an identical dose. The lamp width (100 mm) was

149 smaller than the width of the irradiation chamber window (260 mm) so the lamp power was higher near

150 the center of the irradiation chamber window compared to the edge. The UV sensitive film indicated a

151 power of approximately 120 µW/cm^2 in the center third of the window and 70 µW/cm^2 for the outer

152 thirds. The silicon detector was used to quantify the reflectivity of the aluminum sheet at approximately

153 15% of the incident power. Combining this data allowed the calculation of the average total dose of 2.0

154 mJ/cm^2 to a particle traversing the window in 20 seconds. Additionally, the silicon detector was used to

155 confirm the attenuation of 222-nm light through a single sheet of plastic film was 65%. The addition of

156 one or two sheets of plastic film between the lamps and the irradiation chamber window yielded average

157 doses of 1.3 mJ/cm^2 and 0.8 mJ/cm^2, respectively.

158 **Benchtop aerosol irradiation chamber.** A one-pass, dynamic aerosol / virus irradiation chamber was

159 constructed in a similar configuration to that used by Ko et al.[33], Lai et al.[34], and McDevitt et al.[19,35]. A

160 schematic overview of the system is shown in Fig. 3. Aerosolized viruses were generated by adding a

161   virus solution into a high-output extended aerosol respiratory therapy (HEART) nebulizer (Westmed,

162   Tucson, AZ) and operated using a dual-head pump (Thermo Fisher 420-2901-00FK, Waltham, MA)

163   with an input flow rate of 11 L/min. The aerosolized virus flowed into the irradiation chamber where it

164   was mixed with independently controlled inputs of humidified and dried air. Humidified air was

165   produced by bubbling air through water, while dry air was provided by passing air through a desiccant

166   air dryer (X06-02-00, Wilkerson Corp, Richland, MI). Adjusting the ratio of humid and dry air enabled

167   control of the relative humidity (RH) within the irradiation chamber which, along with the nebulizer

168   settings, determined the aerosol particle size distribution. An optimal RH value of 55% resulted in a

169   distribution of aerosol particle sizes similar to the natural distribution from human coughing and

170   breathing, which has been shown to be distributed around approximately 1 μm, with a significant tail of

171   particles less than 1 μm[36-38].

172   After combining the humidity control inputs with the aerosolized virus, input flow was directed

173   through a series of baffles that promoted droplet drying and mixing to produce an even particle

174   distribution [34]. The RH and temperature inside the irradiation chamber were monitored using an Omega

175   RH32 meter (Omega Engineering Inc., Stamford, CT) immediately following the baffles. A Hal

176   Technologies HAL-HPC300 particle sizer (Fontana, CA) was adjoined to the irradiation chamber to

177   allow for sampling of particle sizes throughout operation.

178   During UV exposure, the three 222-nm lamps with filters were stacked vertically and placed 11

179   cm from the irradiation chamber window. The lamps were directed at the 26 cm × 25.6 cm chamber

180   window which was constructed of 254-μm thick UV transparent plastic film (Topas 8007X10, Topas

181   Advanced Polymers, Florence, KY), and which had a transmission of ~65% at 222 nm. The wall of the

182   irradiation chamber opposite the transparent window was constructed with polished aluminum in order

183   to reflect a portion of the UVC light back through the exposure region, therefore increasing the overall

184 exposure dose by having photons pass in both directions. The depth of the irradiation chamber between

185 the window and the aluminum panel was 6.3 cm, creating a total exposure volume of 4.2 L.

186   Flow of the aerosols continues out of the irradiation chamber to a set of three way valves that

187 could be configured to either pass through a bypass channel (used when no sampling was required), or a

188 BioSampler (SKC Inc, Eighty Four, PA) used to collect the virus. The BioSampler uses sonic flow

189 impingement upon a liquid surface to collect aerosols when operated at an air flow of 12.5 L/min.

190 Finally, flow continued out of the system through a final HEPA filter and to a vacuum pump

191 (WP6111560, EMD Millipore, Billerica, MA). The vacuum pump at the end of the system powered flow

192 through the irradiation chamber. The flow rate through the system was governed by the BioSampler.

193 Given the flow rate and the total exposure volume of the irradiation chamber, 4.2 L, a single aerosol

194 droplet passed through the exposure volume in approximately 20 seconds.

195   The entire irradiation chamber was set up inside a certified class II type A2 biosafety cabinet

196 (Labconco, Kansas City, MO). All air inputs and outputs were equipped with HEPA filters (GE

197 Healthcare Bio-Sciences, Pittsburgh, PA) to prevent unwanted contamination from entering the chamber

198 as well as to block any of the virus from releasing into the environment.

199 **Irradiation chamber performance.** The custom irradiation chamber simulated the transmission of

200 aerosolized viruses produced via human coughing and breathing. The chamber operated at a relative

201 humidity of 55% which resulted in a particle size distribution of 87% between 0.3 μm and 0.5 μm, 11%

202 between 0.5 μm and 0.7 μm, and 2% > 0.7 μm. Aerosolized viruses were efficiently transmitted through

203 the system as evidenced from the control (zero exposure) showing clear virus integration (Fig. 1, top

204 left).

205   **Experimental protocol.** The virus solution in the nebulizer consisted of 1 ml of Dulbecco's Modified

206   Eagle's Medium (DMEM, Life Technologies, Grand Island, NY) containing 10^8 focus forming units per

207   ml (FFU/ml) of influenza A virus [A/PR/8/34 (H1N1)], 20 ml of deionized water, and 0.05 ml of Hank's

208   Balanced Salt Solution with calcium and magnesium (HBSS^{++}). The irradiation chamber was operated

209   with aerosolized virus particles flowing through the chamber and the bypass channel for 15 minutes

210   prior to sampling, in order to establish the desired RH value of ~55%. Sample collection initiated by

211   changing air flow from the bypass channel to the BioSampler using the set of three way valves. The

212   BioSampler was initially filled with 20 ml of HBSS^{++} to capture the aerosol. During each sampling time,

213   which lasted for 30 minutes, the inside of the irradiation chamber was exposed to 222 nm far-UVC light

214   through the UVC semi-transparent plastic window. Variation of the far-UVC dose delivered to aerosol

215   particles was achieved by inserting additional UVC semi-transparent plastic films, identical to the

216   material used as the chamber window, between the lamps and the chamber window. The extra plastic

217   films uniformly reduced the power entering the chamber. The three test doses of 0.8, 1.3 and 2.0

218   mJ/cm^2, were achieved by adding two, one, or no additional plastic films, respectively. Zero-dose

219   control studies were conducted with the excimer lamps turned off. Experiments at each dose were

220   repeated in triplicate. After the sampling period was completed the solution from the BioSampler was

221   used for the virus infectivity assay.

222   **Virus infectivity assay.** We measured viral infectivity with a focus forming assay that employs

223   standard fluorescent immunostaining techniques to detect infected host cells and infectious virus

224   particles[39]. Briefly, after running through the irradiation chamber for 30 minutes, 0.5 ml of virus

225   suspension collected from the BioSampler was overlaid on a monolayer of Madin-Darby Canine Kidney

226   (MDCK) epithelial cells routinely grown in DMEM supplemented with 10% Fetal Bovine Serum (FBS),

227   2 mM L-alanyl-L-glutamine, 100 U/ml penicillin and 100 µg/ml streptomycin (Sigma-Aldrich Corp. St.

11

228   Louis, MO, USA). Cells were incubated with the virus for 45 minutes, washed three times with HBSS^{++}

229   and incubated overnight in DMEM. Infected cells were then fixed in 100% ice cold methanol at 4°C for

230   5 minutes and labeled with influenza A virus nucleoprotein antibody [C43] (Abcam ab128193,

231   Cambridge, MA) 1:200 in HBSS^{++} containing 1% bovine serum albumin (BSA; Sigma-Aldrich Corp.

232   St. Louis, MO, USA) at room temperature for 30 minutes with gentle shaking. Cells were washed three

233   times in HBSS^{++} and labeled with goat anti-mouse Alexa Fluor-488 (Life Technologies, Grand Island,

234   NY) 1:800 in HBSS^{++} containing 1% BSA at room temperature for 30 minutes with gentle shaking.

235   Following three washes in HBSS^{++}, the cells were stained with Vectashield containing DAPI (4',6-

236   diamidino-2-phenylindole) (Victor Laboratories, Burlingame, CA) and observed with the 10x and 40x

237   objectives of an Olympus IX70 fluorescent microscope equipped with a Photometrics PVCAM high-

238   resolution, high-efficiency digital camera. For each sample, at least three fields of view of merged DAPI

239   and Alexa-488 images were acquired. Image-Pro Plus 6.0 software (Media Cybernetics, Bethesda, MD)

240   was used to analyze the 10x images to measure the FFU$_{UV}$ as the ratio of cells infected with the virus

241   divided by the total number of cells.

242   **Data analysis.** The surviving fraction (S) of the virus was calculated by dividing the fraction of cells

243   that yielded positive virus growth at each UV dose (FFU$_{UV}$) by the fraction at zero dose (FFU$_{controls}$):

244   S=FFU$_{UV}$/FFU$_{controls}$. Survival values were calculated for each repeat experiment and natural log (ln)

245   transformed to bring the error distribution closer to normal[40]. Linear regression was performed using

246   these normalized ln[S] values as the dependent variable and UV dose (D, mJ/cm^2) as the independent

247   variable. Using this approach, the virus survival (S) was fitted to first-order kinetics according to the

248   equation[7]:

249    $$\ln[S] = -k \times D \,, \qquad\qquad [1]$$

250   where k is the UV inactivation rate constant or susceptibility factor (cm^2/mJ). The regression was

251   performed with the intercept term set to zero, which represents the definition of 100% relative survival

252   at zero UV dose. Bootstrap 95% confidence intervals for the parameter k were calculated using R 3.2.3

253   software[41]. The virus inactivation cross section, D_{95}, which is the UV dose that inactivates 95% of the

254   exposed virus, was calculated as $D_{95} = -\ln[1-0.95]/k$.

255

References

256

257 1. Wang, H., *et al.* Global, regional, and national life expectancy, all-cause mortality, and cause-
258   specific mortality for 249 causes of death, 1980-2015: A systematic analysis for the Global Burden
259   of Disease Study 2015. *Lancet* **388**, 1459 (2016).

260 2. Paules, C. & Subbarao, K. Influenza. *Lancet* **390**, 697 (2017).

261 3. Cowling, B.J.*, et al.* Aerosol transmission is an important mode of influenza A virus spread. *Nat.*
262   *Commun.* **4**, 1935 (2013).

263 4. Yu, I.T.*, et al.* Evidence of airborne transmission of the severe acute respiratory syndrome virus.
264   *N. Engl. J. Med.* **350**, 1731 (2004).

265 5. Pai, M.*, et al.* Tuberculosis. *Nat. Rev. Dis. Primers* **2**, 16076 (2016).

266 6. Hollaender, A., du Buy, H.G., Ingraham, H.S. & Wheeler, S.M. Control of air-borne
267   microorganisms by ultraviolet floor irradiation. *Science* **99**, 130 (1944).

268 7. Kowalski, W.J. *Ultraviolet Germicidal Irradiation Handbook: UVGI for Air and Surface*
269   *Disinfection* (Springer, Heidelberg: 2009).

270 8. Wells, W.F. & Fair, G.M. Viability of B. Coli exposed to ultra-violet radiation in air. *Science* **82**,
271   280 (1935).

272 9. Conner-Kerr, T.A., Sullivan, P.K., Gaillard, J., Franklin, M.E. & Jones, R.M. The effects of
273   ultraviolet radiation on antibiotic-resistant bacteria in vitro. *Ostom. Wound Manage.* **44**, 50 (1998).

274 10. Budowsky, E.I., Bresler, S.E., Friedman, E.A. & Zheleznova, N.V. Principles of selective
275   inactivation of viral genome. I. UV-induced inactivation of influenza virus. *Arch. Virol.* **68**, 239
276   (1981).

277   11.   Setlow, R.B., Grist, E., Thompson, K. & Woodhead, A.D. Wavelengths effective in induction of

278   malignant melanoma. *Proc. Natl. Acad. Sci. USA* **90**, 6666 (1993).

279   12.   Balasubramanian, D. Ultraviolet radiation and cataract. *J. Ocul. Pharmacol. Ther.* **16**, 285 (2000).

280   13.   Buonanno, M.*, et al.* 207-nm UV light - a promising tool for safe low-cost reduction of surgical

281   site infections. I: In vitro studies. *PLoS One* **8**, e76968 (2013).

282   14.   Buonanno, M.*, et al.* 207-nm UV Light-A Promising tool for safe low-cost reduction of surgical

283   site infections. II: In-vivo safety studies. *PLoS One* **11**, e0138418 (2016).

284   15.   Buonanno, M.*, et al.* Germicidal efficacy and mammalian skin safety of 222-nm UV light. *Radiat.*

285   *Res.* **187**, 483 (2017).

286   16.   Matafonova, G.G., Batoev, V.B., Astakhova, S.A., Gómez, M. & Christofi, N. Efficiency of KrCl

287   excilamp (222 nm) for inactivation of bacteria in suspension. *Lett. Appl. Microbiol.* **47**, 508

288   (2008).

289   17.   Sosnin, E.A., Avdeev, S.M., Kuznetzova, E.A. & Lavrent'eva, L.V. A bactericidal barrier-

290   discharge KrBr excilamp. *Instrum. Experiment. Tech.* **48**, 663 (2005).

291   18.   Wang, D., Oppenländer, T., El-Din, M.G. & Bolton, J.R. Comparison of the disinfection effects of

292   Vacuum-UV (VUV) and UV light on Bacillus Subtilis spores in aqueous suspensions at 172, 222

293   and 254 nm. *Photochem. Photobiol.* **86**, 176 (2010).

294   19.   McDevitt, J.J., Rudnick, S.N. & Radonovich, L.J. Aerosol susceptibility of influenza virus to UV-

295   C Light. *Appl. Environ. Microbiol.* **78**, 1666 (2012).

296   20.   Reed, N.G. The history of ultraviolet germicidal irradiation for air disinfection. *Public Health Rep.*

297   **125**, 15 (2010).

298   21.   Nardell, E., Vincent, R. & Sliney, D.H. Upper-room ultraviolet germicidal irradiation (UVGI) for

299   air disinfection: a symposium in print. *Photochem. Photobiol.* **89**, 764 (2013).

300   22.   Rudnick, S.N.*, et al.* Spatial distribution of fluence rate from upper-room ultraviolet germicidal

301   irradiation: Experimental validation of a computer-aided design tool. *HVAC&R Res.* **18**, 774

302   (2012).

303   23.   Blum, H.E. The human microbiome. *Adv. Med. Sci.* **62**, 414 (2017).

304   24.   Grice, E.A. & Segre, J.A. The skin microbiome. *Nat. Rev. Microbiol.* **9**, 244 (2011).

305   25.   Larson, E.L., Cohen, B. & Baxter, K.A. Analysis of alcohol-based hand sanitizer delivery systems:

306   efficacy of foam, gel, and wipes against influenza A (H1N1) virus on hands. *Am. J. Infect. Control*

307   **40**, 806 (2012).

308   26.   Rahmani, B., Bhosle, S. & Zissis, G. Dielectric-barrier-discharge excilamp in mixtures of krypton

309   and molecular chlorine. *IEEE Trans. Plasma Sci.* **37**, 546 (2009).

310   27.   Sosnin, E.A., Avdeev, S.M., Tarasenko, V.F., Skakun, V.S. & Schitz, D.V. KrCl barrier-discharge

311   excilamps: Energy characteristics and applications. *Instrum. Exp. Tech.* **58**, 309 (2015).

312   28.   Welch, D., Randers-Pehrson, G., Spotnitz, H.M. & Brenner, D.J. Unlaminated gafchromic EBT3

313   film for ultraviolet radiation monitoring. *Radiat. Protect. Dosim.* **In Press**, 10.1093/rpd/ncx016

314   (2017).

315   29.   Welch, D., Spotnitz, H.M. & Brenner, D.J. Measurement of UV emission from a diffusing optical

316   fiber using radiochromic film. *Photochem. Photobiol.* (2017).

317   30.   Drobny, J.G. Dosimetry and Radiometry. In *Radiation Technology for Polymers, Second Edition*

318   215 (CRC Press, 2010).

319   31.   Krins, A., Bolsée, D., Dörschel, B., Gillotay, D. & Knuschke, P. Angular dependence of the

320   efficiency of the UV sensor polysulphone film. *Radiat. Protec. Dosim.* **87**, 261 (2000).

321   32.   Mendez, I., Peterlin, P., Hudej, R., Strojnik, A. & Casar, B. On multichannel film dosimetry with

322   channel-independent perturbations. *Med Phys* **41**, 011705 (2014).

323   33.   Ko, G., First, M.W. & Burge, H.A. Influence of relative humidity on particle size and UV

324   sensitivity of Serratia marcescens and Mycobacterium bovis BCG aerosols. *Tuberc. Lung Disease*

325   **80**, 217 (2000).

326   34.   Lai, K.M., Burge, H.A. & First, M.W. Size and UV germicidal irradiation susceptibility of Serratia

327   marcescens when aerosolized from different suspending media. *Appl. Environ.Microbiol.* **70**, 2021

328   (2004).

329   35.   McDevitt, J.J.*, et al.* Characterization of UVC light sensitivity of Vaccinia virus. *Appl. Environ.*

330   *Microbiol.* **73**, 5760 (2007).

331   36.   Chao, C.Y.H.*, et al.* Characterization of expiration air jets and droplet size distributions

332   immediately at the mouth opening. *J. Aerosol Sci.* **40**, 122 (2009).

333   37.   Papineni, R.S. & Rosenthal, F.S. The size distribution of droplets in the exhaled breath of healthy

334   human subjects. *J. Aerosol Med.* **10**, 105 (1997).

335   38.   Morawska, L.*, et al.* Size distribution and sites of origin of droplets expelled from the human

336   respiratory tract during expiratory activities. *J. Aerosol Sci.* **40**, 256 (2009).

337   39.   Flint, S.J., Racaniello, V.R., Enquist, L.W. & Skalka, A.M. *Principles of Virology, Volume 2:*

338   *Pathogenesis and Control* (ASM Press, Washington DC, Fourth Edition, 2015).

339   40.   Keene, O.N. The log transformation is special. *Stat. Med.* **14**, 811 (1995).

340   41.   Ihaka, R. & Gentleman, R.   R: A Language for Data Analysis and Graphics. *J. Comp. Graph.*

341   *Stat.* **5**, 299 (1996).

342

343

344 **Acknowledgements**

348

349 **Author Contributions**

350 D.W., M.B., and V.G. designed and performed experiments, analyzed the data, and wrote the

351 manuscript; I.S. analyzed the data; C.C. and A.W.B. designed the irradiation chamber; G.W.J.

352 constructed the irradiation chamber; D.J.B and G.R-P. supervised, contributed conceptual advice, and

353 wrote the manuscript. All authors discussed the results and commented on the manuscript.
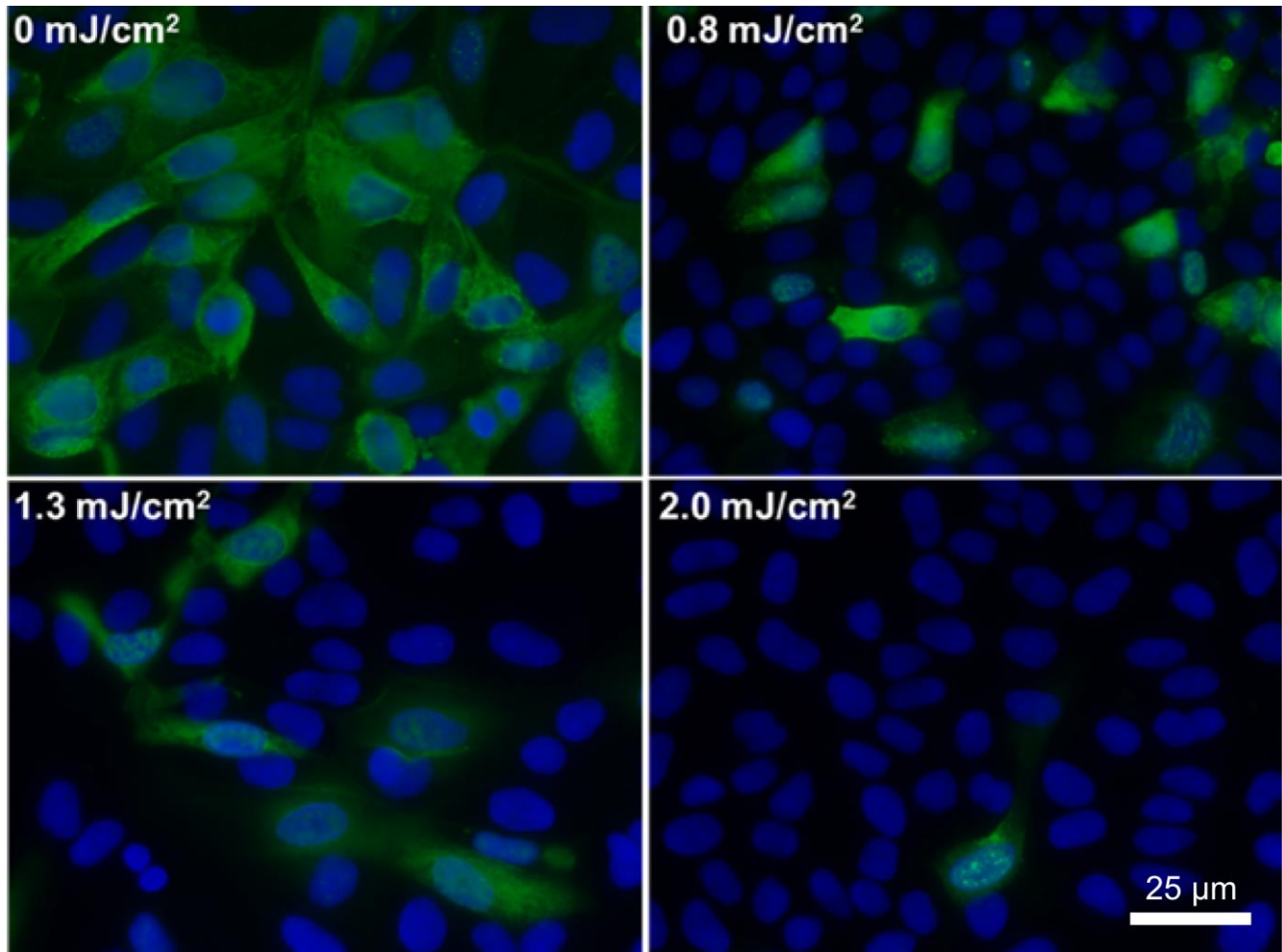
354

355 **Competing Interests**

356 The authors declare that they have no competing interests.

357

358

359

360

361

362

Figure 1 Antiviral efficacy of different low doses of 222-nm far-UVC light. Typical fluorescent images of MDCK epithelial cells infected with influenza A virus (H1N1). The viruses were exposed in aerosolized form in the irradiation chamber to doses of 0, 0.8, 1.3 or 2.0 mJ/cm^2 of 222-nm far-UVC light. Infected cells fluoresce green (blue = nuclear stain DAPI; green= Alexa Fluor-488 conjugated to anti-influenza A antibody). Images were acquired with a 40x objective.
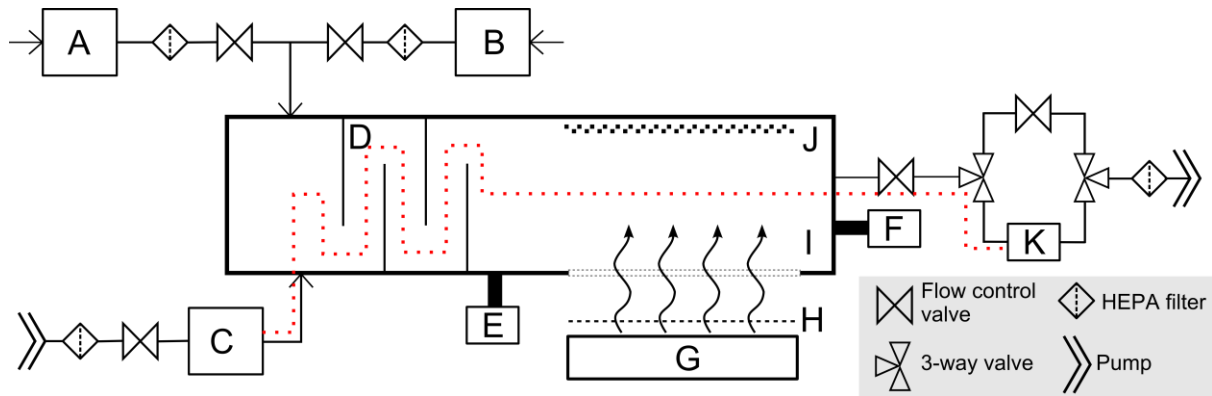
368

369

370

371

372
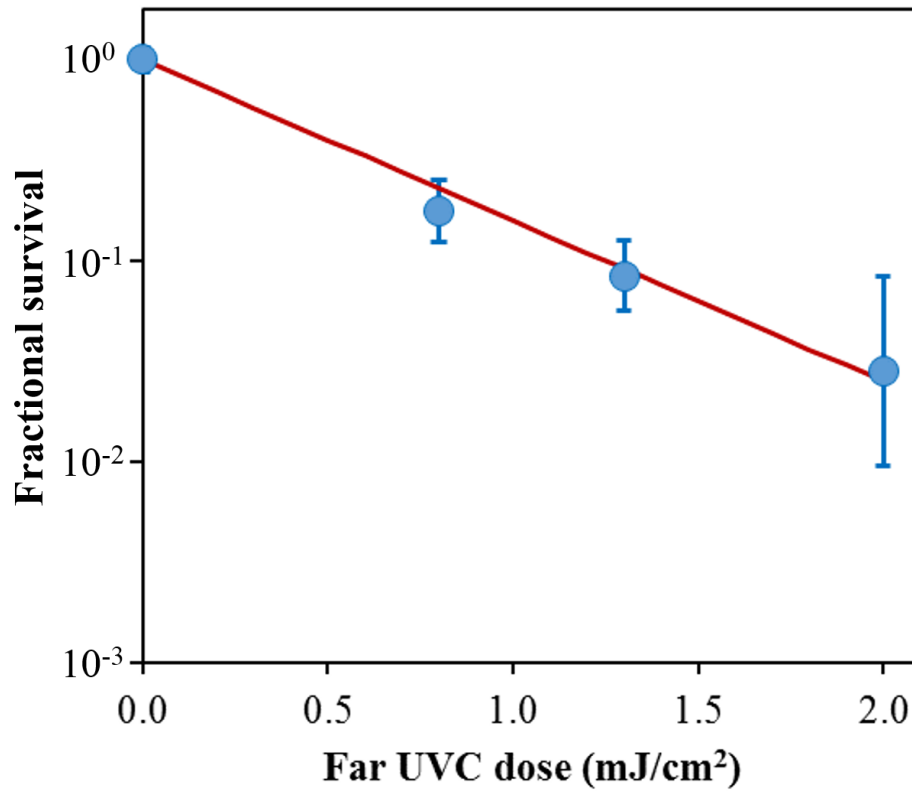
Figure 2   Quantification of the antiviral efficacy of 222-nm far-UVC light. Fractional survival, FFU_{UV} / $FFU_{controls}$, is plotted as a function of the 222-nm far-UVC dose. Means and standard deviations refer to triplicate repeat studies and the line represents the best-fit regression to Eqn 1 (see text).

377

378

379

380

Figure 3 Schematic diagram of the custom UV irradiation chamber. The chamber is depicted in a top down view. Components of the setup include: water bubbler for humidified air input (A), a desiccator for dry air input (B), a nebulizer (C), baffles (D), an RH and temperature meter (E), a particle sizer (F), far-UVC lamps (G), band pass filters (H), a far-UVC transmitting plastic window (I), a reflective aluminum surface (J), and a BioSampler (K). Pumps are used to pressurize the nebulizer for aerosol generation and to control flow through the system. Flow control valves allow adjustments through the system. HEPA filters are included on all air inputs and outputs. A set of three way valves controls flow to or around the BioSampler. The vertically stacked lamps are directed at the window in the side of the chamber to expose the aerosols passing horizontally. The additional films to uniformly decrease the dose were placed between the filters and the window. The path of the aerosolized virus within the system during sampling is indicated with the red dotted line.

392

21